J Stomatol Oral Maxillofac Surg xxx (xxxx) xxx–xxx

Available online at
ScienceDirect
www.sciencedirect.com

Elsevier Masson France
EM|consulte
www.em-consulte.com/en

Original Article

Biomechanical assessment of orbital fractures using patient-specific models and clinical matching

A. Darwich [a,b], A. Attieh [c], A. Khalil [d], S. Szávai [e], H. Nazha [e,*]

[a] Faculty of Biomedical Engineering, Al-Andalus University for Medical Sciences, Tartous, Syria
[b] Faculty of Technical Engineering, University of Tartous, Tartous, Syria
[c] Faculty of Dentistry, Al-Andalus University for Medical Sciences, Tartous, Syria
[d] Faculty of Dentistry, Tishreen University, Lattakia, Syria
[e] Faculty of Mechanical Engineering and Informatics, University of Miskolc, Miskolc, Hungary

ARTICLE INFO

Article history:
Received 14 November 2020
Accepted 28 December 2020

Keywords:
Orbital fractures
Hydraulic mechanism
Buckling mechanism
Finite element analysis

ABSTRACT

Introduction: Orbital wall fractures consider one of the most common fractures in the maxillofacial trauma. These fractures caused by two mechanisms, the buckling mechanism and hydraulic mechanism. This study aims to compare between the two mechanisms in terms of intensity and extension using the finite elements method.
Material and methods: Three-dimensional model of the skull was generated using computed tomography data of young male patient. Virtual loads were applied on the eyeball and the infra-orbital rim separately. Von Mises stresses were examined in each simulation.
Results: The simulation predicted fractures on the infra-orbital rim and orbital floor when simulating the hydraulic mechanism, and on the orbital floor and mesial wall when simulating the buckling mechanism.
Conclusion: Biomechanical studies are essential part in understanding maxillofacial fractures mechanisms. The results confirmed and ascertained what is seen clinically, and explained clearly the two mechanisms of orbital fractures.

1. Introduction

Orbital fractures are common facial fractures in maxillofacial surgery, and they have aesthetic and functional considerations so it is important to understand their mechanisms for effective prevention and treatment [1,2]. Orbital walls fracture happens either isolated which constitute 4–16% of facial fractures, or as part of other fractures like zygomatico-maxillary complex fractures or naso-orbital-ethmoid fractures. The incidence of these fractures approaches 30–55% [3].

Isolated orbital fractures often described by their location and size of the defect. Three patterns of isolated orbital fractures have been described: linear, blow-out, and complex [4]. Zygomatico-maxillary complex fractures are the most common fractures involving orbital fractures. Naso-orbital-ethmoid fractures most often occur blunt trauma to the midface, and usually involve orbital walls fractures [3].

The orbit is shaped like pyramid with its base is formed by the orbital rims anteriorly. The bony orbit is consisted of seven bones: frontal, zygomatic, lacrimal, maxillary, ethmoid, sphenoid, and palatal. It has four walls vary in thickness and strength. Medial wall, which is the thinnest, is composed of sphenoid, lacrimal, and palatal bones. Lateral wall which is composed of zygomatic and sphenoid. Orbital roof is composed of frontal bone and sphenoid bone and it separates the orbit from anterior cranial fossa. In addition, orbital floor is composed of maxillary, zygomatico and palatal bone and it forms the maxillary sinus roof [3]. Orbital floor fractures either solely (blow-out fracture) or as part of zygomatico-maxillary complex (ZMC) fractures.

Several studies have been conducted to illustrate the mechanisms of orbital floor fractures [4,5]. Orbital fractures happen when increased pressure within the components of the orbit causes the fragile walls of the orbit to fracture [6]. In the case of ZMC fractures, infra orbital rim and orbital floor are bend. Medial orbital wall fractures happen either with blow-out fractures, or as part of naso-orbitoethmoid complex fractures [7]. This complex consists of many anatomical structures and it is adjacent to the anterior skull base where fractures extended to this area might have severe

* Corresponding author.
E-mail address: hasan.nazha@uni-miskolc.hu (H. Nazha).

https://doi.org/10.1016/j.jormas.2020.12.008
2468-7855/

consequences [8]. Lateral orbital wall trauma is usually accompanied with ZMC fractures as large part of lateral orbital rim is frontal process of zygoma.

The Zygomatico-Maxillary Complex (ZMC) is a facial bone with a quadruped shape. It articulates with the frontal bone, temporal bone, maxilla, and sphenoid bone, and serves as the main bridge between these bones [9]. It is an aesthetic and functional unit of the facial skeleton. After the nasal bone, they consider the second most commonly fractured sites [10].

Finite element models showed a high degree of success in predicting the biomechanical behavior of skeletal bones such as long bones and iliac [11,12]. This technique relies on replacement of complicated differential equations of irregular shapes with an extensive system of algebraic equations, which represent small geometric entities that can be solved by a computer [13]. In this method, the studied structure is modeled into a mesh of tetrahedral elements that are connected together with nodes. The physical properties of these elements are assigned, a number of these elements are constrained and known forces are applied and the stresses and strains are calculated at each node and in each element [14].

Simulation of facial fractures using finite elements method can help to understand their biomechanical behavior and improves current surgical treatment protocols. The aim of this study is to investigate the biomechanical behavior of orbital walls when sustaining a single load using the finite elements method.

2. Materials and methods

Finite element analysis was used to investigate fracture patterns of orbital walls. The 0.6 mm thickness DICOM files were obtained from CT scanner (Siemens SOMATOM) of 35 years old male patient, where the males from this age range are the most of those exposed to facial trauma [15]. The data was obtained from Radiology Department at Tishreen University Hospital, Lattakia, Syria. Patient approval was taken to use his CT data in this study. DICOM files were imported into MIMICS software (Materialise, inc, Belgium) to Isolate the bone using Tresholding algorithm, build a 3D model of the skull as shown in Fig. 1, and Emit the mandible from the skull because our study focuses on the orbit only.

3-MATIC software (Materialse, inc, Belgium) was used in exporting the 3D model to design a sphere that touches the inner walls of the orbit, thus simulating the eye, mesh the surface, where it was divided into triangular elements connected to each other by nodes (Fig. 2A), Create volume mesh based on the surface mesh (dividing the body into tetrahedral elements that are connected with nodes) which comprised 560,000 elements, and convert 4-noded tetrahedral elements into 10-noded tetrahedral elements which are better for analysis results accuracy.

3-MATIC file (.cdb) was exported to ANSYS software 18.1 (Ansys inc, USA) for finite element analysis as follows: The areas where the loads will be applied were marked (on the infra-orbital, supra-orbital, medial-orbital, lateral-orbital rims and the center of the

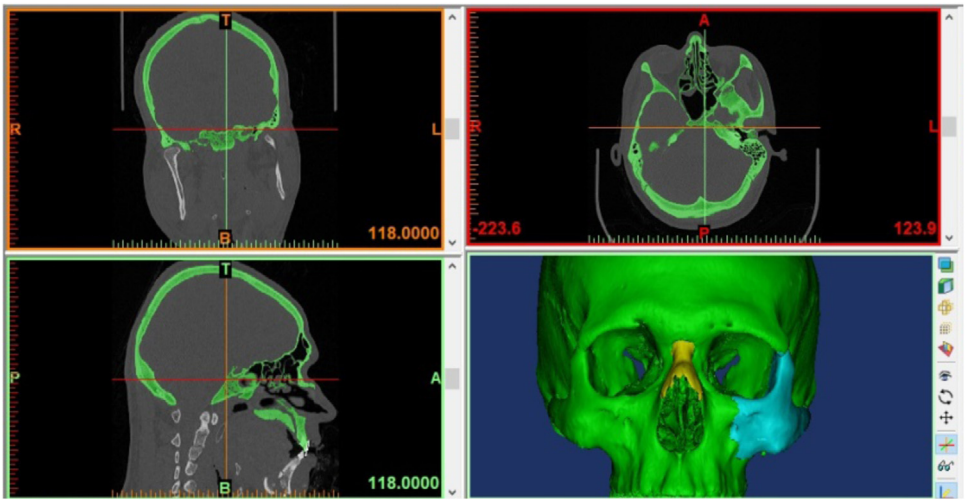

Fig. 1. MIMICS software, used in 3D model construction.

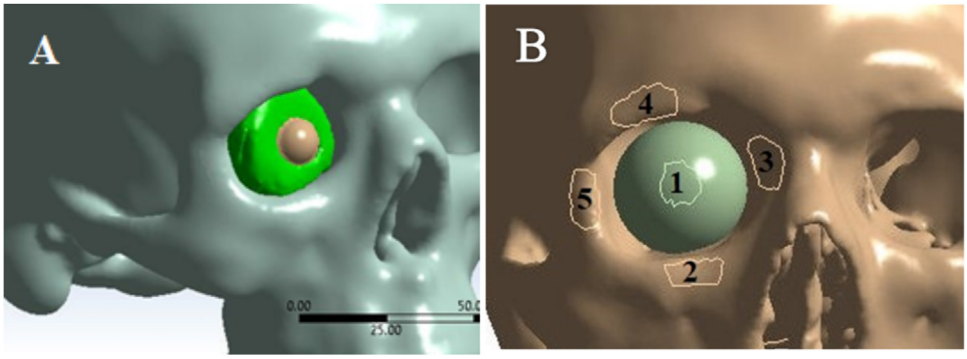

Fig. 2. (A) Skull surface and virtual eyeball and surrounding fat in 3-matic software, (B) marked sites in Ansys where loads was applied.

virtual eyeball) as shown in (Fig. 2B). Mark areas to be constrained (the two occipital condyles of the skull).

Material properties were assigned for both the skull bone and the eyeball (density, Young's modulus and Poisson ratio) as follows: Young modulus was calculated based on density values according to Morgan approach [16]. Each element of the volumetric mesh was assigned with individual values for physical properties, including both density values and Young modulus with the help of APDL Script in ANSYS software. Poisson ratio was assigned to 0.3 according to Huskes [17]. The virtual eyeball was assigned to Young modulus of Water at 2000 MPa due to its high water content, and density of water is known to be 997 kg/m^3 [17]. Poisson ratio of the entire eyeball was obtained from medical literature at 0.47 [18]. The contact surface between skull and virtual eyeball was modeled using coulomb friction model. The coefficient of friction for this contact was defined with 0.3 [19]. Five study designs were chosen to simulate what is seen clinically: Apply load to the virtual eyeball, apply load to the infra-orbital rim, apply load to the medial-orbital rim, apply load to the supra-orbital rim, and apply load to the lateral-orbital rim.

Orbital fat was taken into account as the role of the fat is crucial to explain the hydraulic mechanism of orbital fractures as indicated in Foletti et al. [20]. Virtual static loads were applied in each study design along Y-axis which is perpendicular to the surface on which the load was applied. The load was gradually increased by 100 N at a time until we reached von Mises stress value of 153 MPa or above. When resultant stresses exceeded the value of 153 MPa, the causal load was recorded and simulation was stopped in each design. We assumed that the von Mises stress above 153 MPa was the criteria of failure for skull bones according to Nagasao et al. study [21], where this stress value is when the bone change from the elastic phase to the plastic phase and then begins to fail (fracture). The skull was fixed at the occipital condyles in all degrees of freedom.

3. Results

Von Mises stress was evaluated, which can be used to predict material failure successfully. Results were plotted as color spectrum ranged from blue to red, where red indicates the highest value of calculated stress, and in this study red color indicate that stress has reached the yield strength (153 MPa) at which the bone began to fail (fracture).

3.1. Load on virtual eyeball

It has been found a maximum von Mises stress value of 155 MPa when applying a force of 7200 N on the eyeball along the Y-axis on the marked area as shown in Fig. 3. The analysis results revealed concentration of stresses in the orbital floor and the medial wall of the orbit (Fig. 3), with the highest at the orbital floor indicating that the stresses are approaching or exceeding the 153 MPa threshold, which means we can predict a fracture in this area. Moreover, the presence of orbital fat seemed to increase the force value until the fracture threshold is reached (9000 N). This point out to a significant protective role, which the orbital fat may play. High stresses were concentrated at orbital medial wall and floor; they also spread to skull base without reaching high values as shown in Fig. 3.

3.2. Load on the infra-orbital rim

It has been found a maximum von Mises stress value of 156 MPa when applying load of 8600 N at the infra-orbital rim along the Y-axis on the marked area as shown in Fig. 4.

Simulation revealed concentration of stresses in the infra-orbital rim and front section of the orbital floor, where red spots indicate that the stresses are approaching the threshold of 153 MPa, which means we can predict a fracture in these two

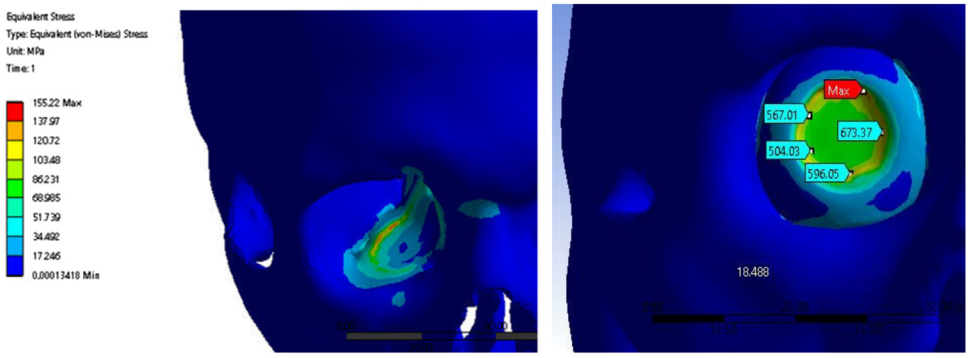

Fig. 3. Concentrations of stresses at orbital floor and orbital mesial wall without (left) and with (right) the presence of orbital fat.

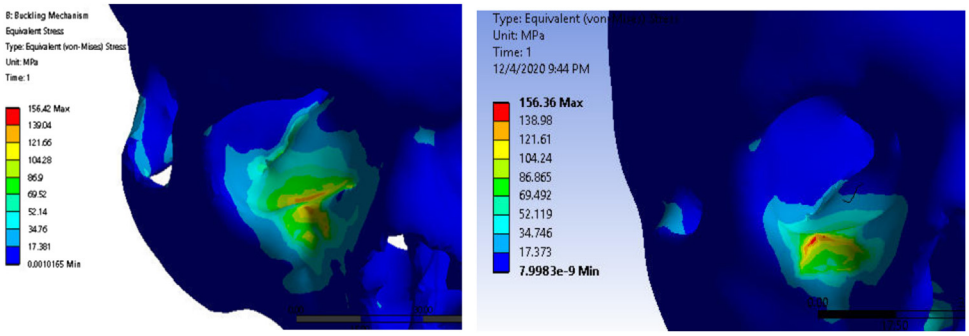

Fig. 4. The distribution of stresses when the force was applied on the infra-orbital rim without (left) and with (right) the presence of orbital fat.

regions as shown in Fig. 4. The presence of orbital fat seems to cause a stress concentration in in the orbital floor and to the maxillary sinus walls and skull base without reaching the 153 MPa threshold as shown in the right shape of Fig. 4.

3.3. Load on medial orbital rim

When simulating a blow on the medial orbital wall, it has been found that von Mises stress value of 154 MPa when applying static load of 5400 N. These stresses were concentrated at site of load and spread to frontal, ethmoidal, and nasal bones. This simulation result is similar to what is found in NOE fractures as shown in Fig. 5. Minimal role of orbital fat has been noticed in this type of loading as similar patterns has appeared with approximative stress values.

3.4. Load on the supra-orbital rim

Gradually increasing loads were (100 N at time) on supra-orbital rim to investigate orbital roof fractures. The maximum von Mises stress value of 153 MPa was found when applying load of 9000 N at the supra-orbital rim along the Y-axis on the pre-defined area Fig. 6. Stresses spread to frontal bone and orbital roof with relatively high values where the highest stress was at the site of load (orbital roof). Stress also spread to temporal bone. The presence of orbital fat caused a slight elevation in stress values and caused in a more expanded fracture pattern at the upper rim as seen in Fig. 6.

3.5. Load on lateral orbital rim

The maximum stress value of 154 MPa was found when applying load of 9300 N at the lateral-orbital rim along the Y-axis on the marked area as shown in Fig. 7. Stresses spread to large areas of the zygomatico-maxillary complex. Minimal role of orbital fat has appeared in this fracture pattern as the shapes and the values were similar.

Simulation shows stress concentration in the lateral orbital wall and rim. The fractures can be predicted fractures in these areas and in the zygomatico-maxillary complex, as the simulation shows in Fig. 7 stress spread to large areas of this complex.

Fig. 8 shows a 19-years old patient with blow-out fracture caused by personal violence, CT scan revealed an orbital floor fracture which is corresponded to our results as shown in the sagittal cross section. Fig. 9 shows the clinical validation of fracture stresses when the force was applied on the lateral-orbital rim.

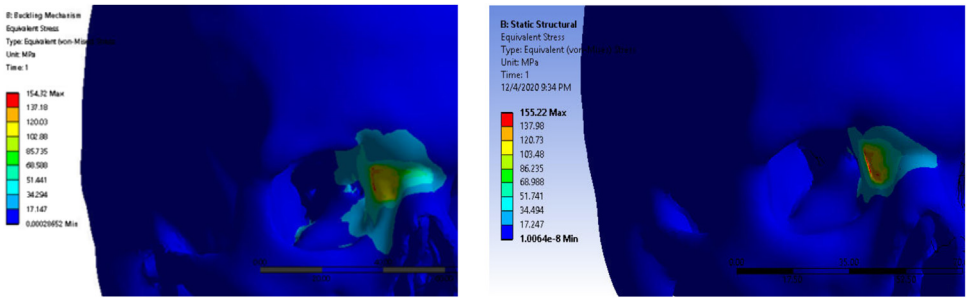

Fig. 5. The distribution of stresses when the force was applied on medial orbital wall without (left) and with (right) the presence of orbital fat.

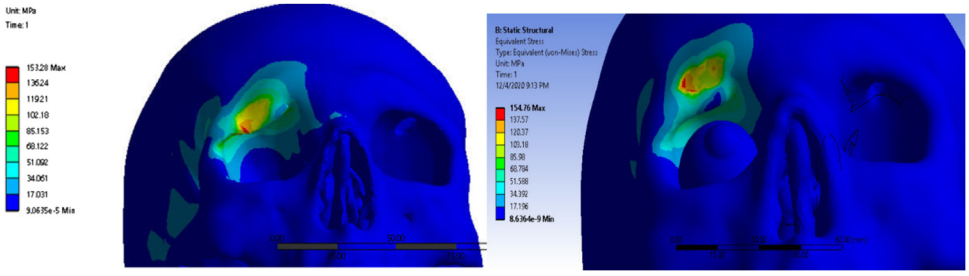

Fig. 6. The distribution of stresses when the force was applied on the supra-orbital rim without (left) and with (right) the presence of orbital fat.

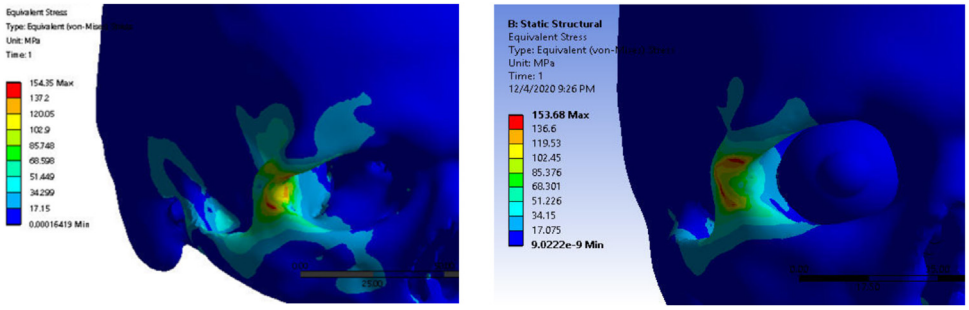

Fig. 7. The distribution of stresses when the force was applied on the lateral-orbital rim without (left) and with (right) the presence of orbital fat.

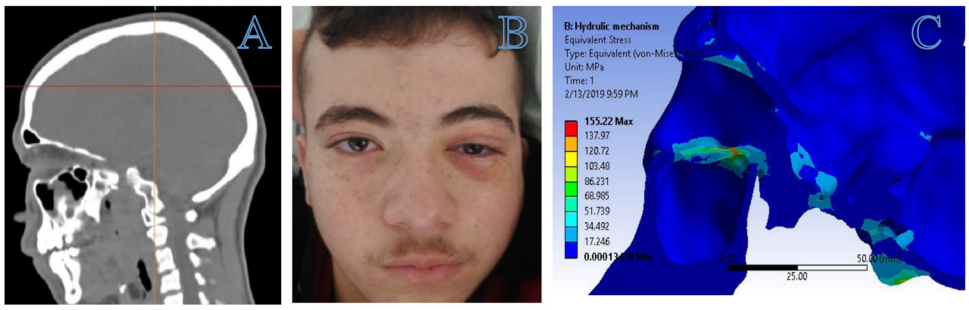

Fig. 8. (A) CT scan revealed an orbital floor fracture, (B) 19-years old patient with blow-out fracture caused by personal violence, (C) the results in the sagittal cross section.

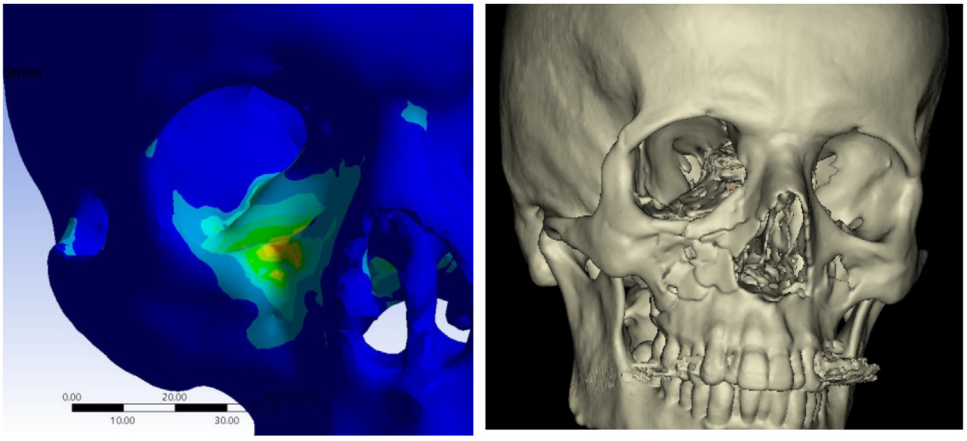

Fig. 9. The clinical validation of fracture stresses when the force was applied on the lateral-orbital rim.

4. Discussion

Orbital walls fractures occur when the traumatic force affects the orbit area in the event of traffic accidents, personal violence, and war injuries [22,23]. Most existing studies on orbital fractures used experimental methods like, hitting skulls with pre-measured objects [4–6,24–27]. However, it is difficult to maintain the continuity of the experiment conditions because these conditions are easily affected by differences in: impact points, angle of the skull or skull stabilization. To solve this problem, the skull was simulated and performed a finite element analysis on it, which allows us to arrange exact experimental conditions including the direction and intensity of impact and the regions to be struck so we used finite element analysis for this study. The simulation was able to be repeated many times in each design until reaching the stress threshold described by Nagasao et al. [21], which is difficult to achieve using experimental methods.

A detailed model of (the skull of young male) was able to be generated with a dense volume mesh of about 560,000 finite elements. Using such dense model, the details of mideface, orbit, surrounding fat were represented in this study. Finite element models showed a high degree of success in predicting the biomechanical behavior of skeletal bones such as long bones and iliac bone [11,12].

Several studies used finite element method to illustrate orbital fractures. Nagasao et al. [21] placed 1085 points on the surface of a dry skull, then the coordinates of the marking points were measured using a 3D scanner, and then they built a 3D model based on the data from the scanner. The model used in this study was based on data from a computed tomography of a 35-years-old male, producing a model that represents the skull well and simulates real anatomy, including the variable bone thickness.

The detailed finite element model used for simulation (560 k elements), the relatively good resolution of bony structures, and material assignment of each region ensure good representation of the skull both anatomically and biomechanically. This good representation ensures good and reliable results.

The first to introduce the buckling mechanism was Le Fort [28]. This mechanism was defined as the transfer of force across the bone from the infra-orbital rim to the orbital floor. This theory was widely accepted as well as the hydraulic mechanism as a cause of orbital wall fractures [29]. Several experimental studies in literature support the buckling mechanism [4–6,24–27] they simulated the fractures of the orbit by dropping a pre-measured weight or hitting the bony orbit using hammer.

Fujino et al. [24] conducted experiments using skulls without the eyes and the contents of the orbit, they hit the skulls on the infra-orbital rim, thus eliminating the influence of the hydraulic mechanism, focusing on the buckling mechanism [25]. Waterhouse et al. [5] also developed a new device that allows a point-based impact to a specific area of the orbit. Using this device, and striking the eyeball or the infra-orbital rim on skulls individually, they illustrated the fracture patterns for both mechanisms.

Several studies simulated orbital wall fractures based on different numerical environments and under different both static and dynamic scenarios. Takizawa et al. tried to explain orbital fractures, especially the dynamic characteristics of the orbit at the time of the fracture. They analyzed the degree and concentration of stress within the orbit depending on the applied loads, and they found that direct force applied against the inferior orbital rim resulted in increased stress within the lower wall of the orbit, and that stress tends to concentrate in the thin nasal side of the orbital groove as pressure within the orbit mounts [30].

The mechanical response of our skull model was compared with the results of similar literature studies. The current study differs from the study of Nagasao et al. in which the skull model was divided into several triangular parts of different thicknesses, while the model in the current study was based on CT images. This allowed to accurately detect the borders and to produce the thickness of different areas of the skull [21].

On the other hand, and in contrast to the study of Nagasao et al. in which the number of finite elements within the skull model was 248,000, the number of these elements in the model studied in this paper was equal to 560,000 elements, which would produce stress values with a higher spatial accuracy [21].

This number of elements was determined based on the results of Taddei group research which carried out a numerical approach to analyze the influence of the number of finite elements on numerical results. From another side, high resolution results should be discussed more specifically, as images accuracy of 1 mm thickness necessitates modifying the image segmentation manually in order to preserve the continuity shape of the bone, especially in the regions of orbital and ethmoid bones, in which the thickness of orbital wall is approximately equal to 2.27 mm [31].

Our hit oriented to the infra-orbital rim revealed a fracture in the infra-orbital rim and the orbital floor, which corresponds to the experimental model developed by Waterhouse et al. [5]. Our fracture pattern corresponds also with the results of Nagasao and Miyamoto study [21], where they found that fracture occurs in the weakest parts of orbit (orbital floor).

Schaller et al. modeled three different fracture mechanisms based on finite element analysis. A finer skeletal model and a transient dynamic simulation were used to test pure hydraulic, pure buckling and a mixed force transmission, and they found that the role of those mechanisms in explaining the variety of clinical fracture situations [32]. In this concern, our results of eye-ball hit seems to be similar. We found concentration of stresses on the walls of orbit with the greatest at the orbital floor, which simulates a blow-out fracture in both the mesial wall and orbital floor, which is often seen clinically in patients with this type of trauma (Fig. 8).

Kosowski et al. presented initial results of finite element analysis of a blow-out type trauma of orbital wall. This study simulated the tests achieved in laboratories. In the finite element analysis the neighborhood of orbital wall is modelled by triangle thin shell finite elements, and the results of nonlinear static and transient dynamic analysis were compared [33].

Foletti et al. developed a clinically proven finite element model (FEM) of the human orbit in order to study stress behavior under different blunt traumas. Mesh production, and model properties were used to perform blunt trauma simulations based on a 3D FEM comprising of 640 000 elements. Fracture patterns were explained based on buckling and hydraulic theories of orbital floor fractures. This study pointed out to the greatest role of the surrounding fat in varying facture patterns, which may change our knowledge in deciding about the real factors causing the fractures [20].

Our results appeared to be similar to Huempfner-Hierl study investigating Naso-orbito-ethmoid fractures using finite element method [10], where he found similar results when hitting the medial third of the infra-orbital rim with impactor. This result also corresponds to what is seen clinically as shown in Fig. 8.

Trzebiatowski et al. used 2 different three-dimensional finite element method (FEM) models of the human orbital region to simulate the pure ''buckling'' mechanism of orbital wall fracture in two variants: the model of orbital bone elements and the model of orbital bone, orbit and intraorbital tissue elements. A nonlinear transient analysis of the contact problem between bodies that differ substantially in terms of the Young's modulus was carried out to investigate the interaction of different bodies within an instant injury. Potential damage areas were found within the lower orbital wall and these were validated against real injuries [34].

Fracture patterns corresponded with zygomatico-maxillary fractures, and it is similar to what is seen clinically as shown in Fig. 9. The results of the study can be used to predict the risk of blow-out fractures during clinical trials. Modeling orbital contents (muscles and fat) and the soft tissue covering the bone will increase the accuracy of the results, This consideration should be taken into account in the future when better computer capabilities and more advanced computed tomography is available, allowing the modeling of the orbital contents separately.

Compared to the numerical results of Nagasao et al., the fracture pattern resulting from this study is identical to the numerical fracture model distributed through the orbital floor in response to the load applied on the suborbital rim even at low weights of the impact part [21].

In the second model including the effect of the hydraulic theory highlighted by a direct hit on the eyeball, it can be considered that fracture pattern and stress lines are correct based on the latest theoretical and clinical studies [20,31,32]. The fracture model obtained in the current study can be compared to the results obtained by Foletti et al. although the force values is greater than the force cited in this study [20].

Transferring this knowledge to the clinical practice may help in understanding the relationship between the direction of the applied force and the resulting fracture, such as bottom-directed loads can result several periorbital traumas with fewer impacts on the posterior side of the orbital floor.

5. Conclusion

Biomechanical testing has proven to be appropriate in answering questions regarding fracture mechanisms. Our results confirmed what is seen clinically and explained the mechanisms of orbital walls fractures. The results also can help to optimize fracture therapies and improve their outcomes. These simulations help in investigating trauma scenarios and mechanism, which could be useful in forensic sciences.

Conflict of interest

All authors were fully involved in the study and preparation of the manuscript and declare that there is no conflict of interest.

Acknowledgment

The authors are grateful for University of Miskolc (Institute of Machine and Product Design) for its unlimited support.

References

[1] Kaufman Y, Stal D, Cole P, Hollier Jr L. Orbitozygomatic fracture management. Plast Reconstr Surg 2008;121:1370–4. http://dx.doi.org/10.1097/01.prs.0000308390.64117.95.
[2] Suzuki H, Furukawa M, Takahashi E, Matsuura K. Barotraumatic blowout fracture of the orbit. Auris Nasus Larynx 2001;28:257–9. http://dx.doi.org/10.1016/S0385-8146(00)00122-X. 2001.
[3] Fonseca RJ. Oral and maxillofacial trauma, 13. Elsevier Saunders; 2005. p. 316–9. i9780721601830.
[4] Green Jr RP, Peters DR, Shore JW, Fanton JW, Davis H. Force necessary to fracture the orbital floor. Ophthal Plast Reconstr Surg 1990;6:211–7. http://dx.doi.org/10.1097/00002341-199009000-00012.
[5] Waterhouse N, Lyne J, Urdang M, Garey L. An investigation into the mechanism of orbital blowout fractures. Br J Plast Surg 1999;52:607–12. http://dx.doi.org/10.1054/bjps.1999.3194.
[6] Rhee JS, Kilde J, Yoganadan N, Pintar F. Orbital blowout fractures: experimental evidence for the pure hydraulic theory. Arch Facial Plast Surg 2002;4:98–101. http://dx.doi.org/10.1001/archfaci.4.2.98.
[7] Kelley P, Crawford M, Higuera S, Hollier LH. Two hundred ninety-four consecutive facial fractures in an urban trauma center: lessons learned. Plast Reconstr Surg 2005;116:42–9. http://dx.doi.org/10.1097/01.prs.0000177687.83247.27.

[8] Huempfner-Hierl H, Schaller A, Hemprich A, Hierl T. Biomechanical investigation of naso-orbitoethmoid trauma by finite element analysis. Br J Oral Maxillofac Surg 2014;52:850–3. http://dx.doi.org/10.1016/j.bjoms.2014.07.255.
[9] Ahn HC, Youn DH, Choi MSS, Chang JW, Lee JH. Wire or hook traction for reducing zygomatic fracture. Arch Craniofacial Surg 2015;16:131–5. http://dx.doi.org/10.7181/acfs.2015.16.3.131.
[10] Gomes PP, Passeri LA, de Albergaria Barbosa JR. A 5-year retrospective study of zygomatico-orbital complex and zygomatic arch fractures in Sao Paulo State. Brazil. J Oral Maxillofac Surg 2006;64:63–7. http://dx.doi.org/10.1016/j.joms.2005.09.012.
[11] Ramos A, Simoes JA. Tetrahedral versus hexahedral finite elements in numerical modelling of the proximal femur. Med Eng Phys 2006;28:916–24. http://dx.doi.org/10.1016/j.medengphy.2005.12.006.
[12] Anderson AE, Peters CL, Tuttle BD, Weiss JA. Subject-specific finite element model of the pelvis: development, validation and sensitivity studies. J Biomech Eng 2005;127:364–73. http://dx.doi.org/10.1115/1.1894148.
[13] Shash M, Nazha H, Abbas W. Influence of different abutment designs on the biomechanical behavior of one-piece zirconia dental implants and their surrounding bone: a 3D-FEA. IRBM 2019;40:313–9. http://dx.doi.org/10.1016/j.irbm.2019.07.001.
[14] Darwich MA, Albogha MH, Abdelmajeed A, Darwich K. Assessment of the biomechanical performance of 5 plating techniques in fixation of mandibular subcondylar fracture using finite element analysis. J Oral Maxillofac Surg 2016;74:794–801. http://dx.doi.org/10.1016/j.joms.2015.11.021.
[15] Elhammali N, Bremerich A, Rustemeyer J. Demographical and clinical aspects of sports-related maxillofacial and skull base fractures in hospitalized patients. Int J Oral Maxillofac Surg 2010;39:857–62. http://dx.doi.org/10.1016/j.ijom.2010.04.006.
[16] Morgan EF, Bayraktar HH, Keaveny TM. Trabecular bone modulus–density relationships depend on anatomic site. J Biomech 2003;36:897–904. http://dx.doi.org/10.1016/S0021-9290(03)00071-X.
[17] Hulskes R. Finite element analysis of acetabular reconstruction: noncemented threaded cups. Acta Orthop Scand 1987;58:620–5. http://dx.doi.org/10.3109/17453678709146499.
[18] Uchio E, Ohno S, Kudoh J, Aoki K, Kisielewicz LT. Simulation model of an eyeball based on finite element analysis on a supercomputer. Br J Ophthalmol 1999;83:1106–11. http://dx.doi.org/10.1136/bjo.83.10.1106.
[19] Tensi HM, Gese H, Ascherl R. Non-linear three-dimensional finite element analysis of a cementless hip endoprosthesis. Proceedings of the Institution of Mechanical Engineers Part H: Journal of Engineering in Medicine 1989;203:215–22. http://dx.doi.org/10.1243/PIME_PROC_1989_203_042_01.
[20] Foletti JM, Martinez V, Graillon N, Godio-Raboutet Y, Thollon L, Guyot L. Development and validation of an optimized finite element model of the human orbit. J Stomatol Oral Maxillofac Surg 2019;120:16–20. http://dx.doi.org/10.1016/j.jormas.2018.09.002.
[21] Nagasao T, Miyamoto J, Nagasao M, Ogata H, Kaneko T, Tamaki T, et al. The effect of striking angle on the buckling mechanism in blowout fracture. Plast Reconstr Surg 2006;117:2373–80. http://dx.doi.org/10.1097/01.prs.0000218792.70483.1f.
[22] Shere JL, Boole JR, Holtel MR, Amoroso PJ. An analysis of 3599 midfacial and 1141 orbital blowout fractures among 4426 United States Army Soldiers, 1980–2000. Otolaryngol Head Neck Surg 2004;130:164–70. http://dx.doi.org/10.1016/j.otohns.2003.09.018.
[23] Agir H, Ustundag E, Iscen D. Bilateral isolated orbital blowout fractures among terrorist bombing victims. A very rare entity. J Plast Reconstr Aesthetic Surg 2006;59:306–7. http://dx.doi.org/10.1016/j.bjps.2005.09.025.
[24] Fujino T, Sugimoto C, Tajima S, Moribe Y, Sato TB. Mechanism of orbital blowout fracture. Keio J Med 1974;23:115–24. http://dx.doi.org/10.2302/kjm.23.115.
[25] Tajima S, Fujino T, Oshiro T. Mechanism of orbital blowout fracture. Keio J Med 1974;23:71–5. http://dx.doi.org/10.2302/kjm.23.7.
[26] Ahmad F, Kirkpatrick WNA, Lyne J, Urdang M, Garey LJ, Waterhouse N. Strain gauge biomechanical evaluation of forces in orbital floor fractures. Br J Plast Surg 2003;56:3–9. http://dx.doi.org/10.1016/S0007-1226(02)00467-8.
[27] Ahmad F, Kirkpatrick NA, Lyne J, Urdang M, Waterhouse N. Buckling and hydraulic mechanisms in orbital blowout fractures: fact or fiction? J Craniofac Surg 2006;17:438–41. http://dx.doi.org/10.1097/00001665-200605000-00009.
[28] Le Fort R. Etude experimentale sur les fractures de la machoire superieure. Revue Chirurgio 1901;23:208–27. doi: ci.nii.ac.jp/naid/10016046255.
[29] Smith B, Regan WF. Blow-out fracture of the orbit: mechanism and correction of internal orbital fracture. Am J Ophthalmol 1957;44:733–9. http://dx.doi.org/10.1016/0002-9394(76)90774-1.
[30] Takizawa Y, Takahashi K. Three-dimensional finite element analysis of blow-out fractures. Journal of Japanese Ophthalmological Society 1995;99:972–9.
[31] Taddei F, Pancanti A, Viceconti M. An improved method for the automatic mapping of computed tomography numbers onto finite element models. Med Eng Phys 2004;26:61–9. http://dx.doi.org/10.1016/S1350-4533(03)00138-3.
[32] Schaller A, Huempfner-Hierl H, Hemprich A, Hierl T. Biomechanical mechanisms of orbital wall fractures - A transient finite element analysis. J Cranio-maxillofacial Surg 2013;41:710–7. http://dx.doi.org/10.1016/j.jcms.2012.02.008.
[33] Kłosowski P, Skorek A, Trzebiatowski MZ. Static and dynamic modelling blow-out type trauma of orbital wall. In: Shell Structures: Theory and Applications - Proceedings of the 10th SSTA 2013 Conference; 2014;347–50. http://dx.doi.org/10.1201/b15684-86.
[34] Trzebiatowski MAZ, Kłosowski P, Skorek A, Żerdzicki K, Lemski P, Koberda M. Nonlinear dynamic analysis of the pure "buckling" mechanism during blow-out trauma of the human orbit. Sci Rep 2020;10:1–13. http://dx.doi.org/10.1038/s41598-020-72186-1.